

Untied Ulysses: Memory-Efficient Context Parallelism via Headwise Chunking

Ravi Ghadia¹ Maksim Abraham¹ Sergei Vorobyov¹ Max Ryabinin¹

Abstract

Efficiently processing long sequences with Transformer models usually requires splitting the computations across accelerators via context parallelism. The dominant approaches in this family of methods, such as Ring Attention or DeepSpeed Ulysses, enable scaling over the context dimension but do not focus on memory efficiency, which limits the sequence lengths they can support. More advanced techniques, such as Fully Pipelined Distributed Transformer or activation offloading, can further extend the possible context length at the cost of training throughput. In this paper, we present **UPipe**, a simple yet effective context parallelism technique that performs fine-grained chunking at the attention head level. This technique significantly reduces the activation memory usage of self-attention, breaking the activation memory barrier and unlocking much longer context lengths. Our approach reduces intermediate tensor memory usage in the attention layer by as much as **87.5%** for 32B Transformers, while matching previous context parallelism techniques in terms of training speed. UPipe can support the context length of **5M** tokens when training Llama3-8B on a single 8×H100 node, improving upon prior methods by over **25%**.

1. Introduction

The Transformer architecture (Vaswani et al., 2017) has powered significant advances in AI in recent years, ranging from language models with agentic and reasoning capabilities (Gemini Team, 2025; Kimi Team et al., 2025; Chen et al., 2025) to video generation (Team Wan et al., 2025; Wu et al., 2025; Sand.ai et al., 2025). As the field continues to progress, the demand for longer context lengths in AI models continues to grow due to applications such as code generation (Li et al., 2023a; Hui et al., 2024), long document understanding (Chia et al., 2024; Jiang et al., 2024), or

¹Together AI. Correspondence to: Ravi Ghadia <rghadia@together.ai>, Max Ryabinin <mryab@together.ai>.

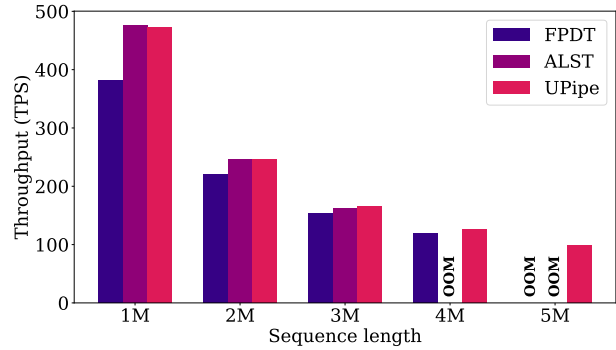


Figure 1. Comparison of context parallelism approaches on long-sequence training for Llama 3-8B using 8 × H100s. UPipe provides maximum efficiency, resulting in longer maximum context length (5M tokens) while retaining throughput.

even audio processing (Hori et al., 2021). However, training models to effectively process such long sequences is limited by the accelerator hardware: beyond a certain limit, even keeping the activations necessary for self-attention becomes a bottleneck. As a result, methods that reduce the memory requirements of long-context training have recently attracted a surge of research interest.

The most scalable approaches for increasing the context size beyond a single accelerator leverage distributed training, splitting the computations and memory allocations across multiple devices. In particular, the context parallelism (Li et al., 2022; 2023b; Jacobs et al., 2023) family of methods (also known as sequence parallelism) focuses on sharding model operations across the sequence axis. These methods enable effective scaling in context length with the number of accelerators, but the activation memory per device still scales linearly with the sequence length. Therefore, at very long sequence lengths (>2M), the activation memory starts to become a bottleneck, limiting the training capacity.

In this paper, we propose **UPipe**, a context parallelism method that focuses on improving the memory efficiency of long-context training while maintaining the performance on par with current approaches. Our method is designed on the principle that for long-context training, processing a subset of heads at once is enough to saturate the GPU. Therefore, serializing the execution in the attention layer by grouping heads into smaller chunks allows for much better memory reuse. UPipe is agnostic to the underlying attention

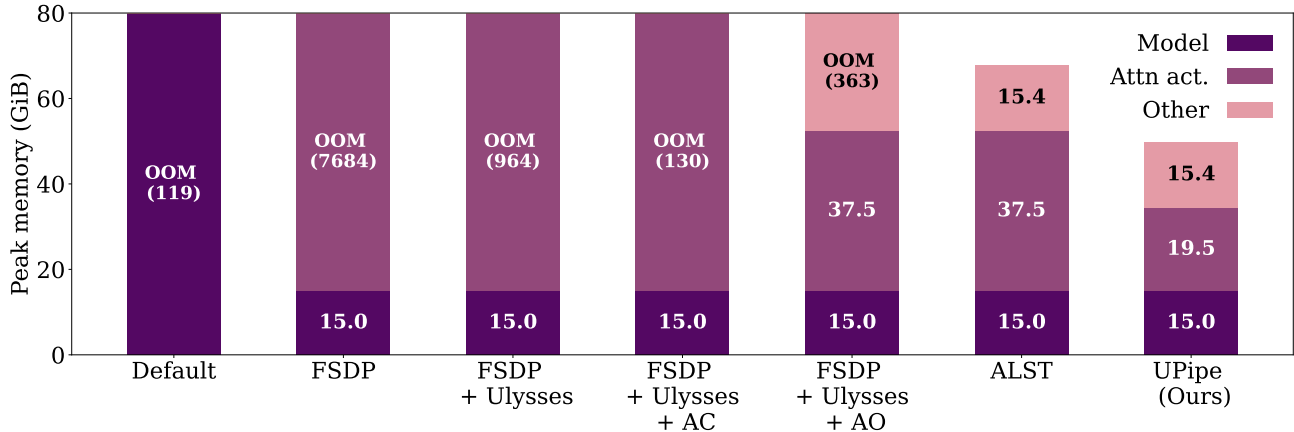


Figure 2. Memory usage breakdown when training Llama3-8B with a sequence length of 3M tokens across 8 H100 GPUs. AC stands for Activation Checkpointing, AO denotes AC with offloading, OOM stands for Out of Memory.

algorithm: similarly to DeepSpeed Ulysses, it uses the same kernels to compute attention as non-distributed training.

On Llama 3-8B, our method is able to fit context lengths of **up to 5 million tokens on a single H100 node**, and up to 8M on two H100 nodes with unified sequence parallelism (Fang & Zhao, 2024), outperforming prior works by **25%** and **33%** respectively in terms of maximum context length supported. At the same time, UPipe’s training throughput is comparable to other context parallelism techniques.

Our contributions are as follows:

1. We propose UPipe, a new context parallelism method that executes the attention layer in multiple stages, processing attention heads in chunks. This method is easy to implement and can work as a plug-and-play replacement for existing techniques.
2. We analyze the memory usage of long-context Transformer training, identifying the major bottleneck left unaddressed by prior works and showing how UPipe mitigates this bottleneck.
3. We present a GQA-compatible schedule for UPipe, which processes heads out of order to avoid redundant communication while retaining the memory benefits of standard GQA architecture.
4. We compare UPipe with prior approaches to context-parallel training, measuring the speed and memory usage for 8B and 32B dense Transformer models across sequence lengths ranging from 128k to 5M tokens¹. UPipe can support longer sequence lengths (up to 5 million tokens on a single 8×H100 node) with negligible performance differences compared to other techniques.

¹The code for our experiments is available at github.com/togethercomputer/Untied-Ulysses.

2. Background

Large language models (LLMs) excel at processing textual information and solving a wide variety of tasks. The research community has also become significantly interested in improving the long context understanding abilities of Transformer-based models for various use cases, such as voice (Yang et al., 2024) and video generation (Sand.ai et al., 2025). However, the paradigm of using regular self-attention for long-sequence data has several obstacles to further scaling. For instance, Team Wan et al. (2025) mention that the memory bottleneck due to activation memory when training a 14B Diffusion Transformer on a sequence length of 1M tokens is 8 TB. It is impossible for a single accelerator to hold such tensors, which necessitates the use of scalable approaches that rely on distributed training.

2.1. Context Parallelism

To mitigate the problem of large activation memory footprint, context parallelism was first introduced by Li et al. (2023b) and later an online softmax compatible version by Liu et al. (2023) via Ring Attention. This allows sharding the context across C devices. Since attention computation requires every shard to attend to other shards, this method first performs a local attention using the local Q, K, V shards present on the device, and then exchanges the K, V shards among the devices in a ring fashion via peer-to-peer communication. Because of this, Ring Attention requires $\mathcal{O}(C)$ communication calls per attention operation, which is expensive in terms of run time. DeepSpeed-Ulysses (Jacobs et al., 2023) is another context parallelism technique built upon Megatron-SP (Korthikanti et al., 2022) that mitigates the runtime overhead by rearranging the tensors via all-to-all, having constant communication volume and unlocking the use of optimized self-attention kernels. We discuss this technique in more detail in Section 3.1.

Table 1. Theoretical peak memory usage breakdown across different stages of the forward pass for a Transformer model. All floating point tensors use `BF16` precision by default, except cross-entropy loss, which uses `FP32` precision.

Stage	Inputs	Intermediate tensors			Outputs	Total
		Type	Memory	Ratio		
❶ Embedding	$4 \cdot S \cdot (\text{int}32)$	–	–	–	$2 \cdot S \cdot d_{model}$	$2 \cdot S \cdot d_{model}$
❷ Attention	$2 \cdot S \cdot d_{model}$	QKV all-to-all	$6 \cdot S \cdot H \cdot d_{head}$ $6 \cdot S \cdot H \cdot d_{head}$	$H = d_{model}/d_{head}$	$2 \cdot S \cdot d_{model}$	$16 \cdot S \cdot d_{model}$
❸ Feed-forward	$2 \cdot S \cdot d_{model}$	Intermediate	$8 \cdot S \cdot d_{ff}$	$d_{ff} \approx 2.67 \cdot d_{model}$	$2 \cdot S \cdot d_{model}$	$25 \cdot S \cdot d_{model}$
❹ Cross-Entropy	$2 \cdot S \cdot d_{model}$	Logits + LogSoftmax	$8 \cdot S \cdot V$	$V \approx 30 \cdot d_{model}$	Loss	$240 \cdot S \cdot d_{model}$

Further works introduce additional optimizations for memory and throughput. For instance, USP (Unified Sequence Parallelism, Fang & Zhao, 2024) uses DeepSpeed-Ulysses within the node and Ring Attention across nodes, running all-to-all communication over the faster NVLink fabric and ring communication over the slower one. To address the memory bottleneck of very long contexts, other papers have explored tiling or chunking techniques. In particular, Arctic Long Sequence Training (ALST, Bekman et al., 2025) uses tiling for feed-forward layer and cross-entropy loss calculations, lowering the memory pressure of intermediate tensors. However, it does not address the memory overhead in the attention phase. Fully Pipelined Distributed Transformer (FPDT, Yao et al., 2025) addresses the memory overhead in self-attention by chunking computations along the sequence length dimension and offloading to CPU. However, it suffers from reduced performance due to CPU overhead and additional memory transfers. UPipe addresses the memory overhead while maintaining performance and extends to hybrid schemes such as USP. Also, our technique performs chunking along the head dimension, which is orthogonal and complementary to the optimizations of FPDT.

2.2. Activation memory for a Transformer model

Next, we quantify and analyze the memory usage in each phase of a long-context Transformer training step. We identify the factors that impose the biggest memory bottlenecks and cover the techniques to address them.

Consider a decoder-only Transformer with L layers, with H heads per layer, and a GQA group size of G . Let the model’s hidden size be d_{model} , per-head dimension d_{head} , the intermediate dimension of the feed-forward network d_{ff} and the vocab size of the model V . Finally, let a sequence of length S be the input to the model. For now, we keep the batch size equal to 1, since our focus is to establish how memory scales with respect to the sequence length S .

We assume a mixed precision setup with parameters, activations and gradients in `bf16` precision, thus requiring 2 bytes per parameter for each tensor. However, some intermediate tensors still require 4 bytes, as discussed below.

For a decoder-only Transformer model, the sequence of operations during the forward pass can be broken down into 4 phases, as shown in Table 1.

❶ **Embedding:** The input sequence of tokens is converted into embedding vectors of size $S \cdot d_{model}$, thus requiring $2 \cdot S \cdot d_{model}$ bytes of memory.

❷ **Attention:** The input gets transformed into query Q , key K and value V vectors, requiring $6 \cdot S \cdot H \cdot d_{head}$ bytes. As we will discuss in Section 3.1, all-to-all requires the same amount of additional memory. Assuming Flash Attention (Dao et al., 2022) is used, the attention computation would not require any additional GPU HBM memory, except for storing the final output (and the final log-sum-exponent) vectors of size $2 \cdot S \cdot d_{model}$ (and $2 \cdot S \cdot H$ respectively). Typically, for most Transformer models, $H = d_{model}/d_{head}$, therefore this phase has a total memory usage of $2 + (6 + 6) + 2 = 16 \cdot S \cdot d_{model}$ bytes.

❸ **FFN:** Next, the attention output is fed to the feed-forward network with two layers, which projects the input with dimension d_{model} into four intermediate tensors (assuming SwiGLU) of dimension d_{ff} and then projects the intermediate tensors into the output of dimension d_{model} . Typically, $d_{ff} \approx 2.67 \cdot d_{model}$, which results in the total memory usage of $25 \cdot S \cdot d_{model}$ bytes.

❹ **Cross-Entropy Loss:** At the end of the final layer, the output is converted into logits of shape $S \cdot V$, which are then used by the cross-entropy loss function. This phase has the most critical memory constraints, because the vocabulary size V is typically very large ($\approx 30 \cdot d_{model}$). Moreover, the cross-entropy calculation requires logits and intermediate log-softmax values to be casted to `fp32`, making the overall memory consumption $240 \cdot S \cdot d_{model}$ bytes.

2.3. Mitigating memory overheads

From the above analysis, we can identify the most critical factors that become a memory bottleneck when scaling the context length. Due to its memory consumption, the cross-entropy loss is the first obstacle. We can overcome it by computing the loss in a tiled manner, materializing

Table 2. Peak activation memory within the forward attention block under GQA. π represents the number of chunks in FPDT, ν represents the number of chunks in UPipe. UPipe consumes ν times less intermediate (QKV + all-to-all) tensor memory than Ulysses + offloading. FPDT has lower memory usage due to arbitrary chunk size, but suffers from performance degradation.

Method	Before attn block	During inp_all_to_all	During attn kernel	During out_all_to_all
Ulysses	$L \cdot \frac{S}{C}$	$L \cdot \frac{S}{C} + (\gamma + 1) \frac{S}{C}$	$L \cdot \frac{S}{C} + (\gamma + 1) \frac{S}{C}$	$L \cdot \frac{S}{C} + 2 \frac{S}{C}$
Ulysses + offloading	$\frac{S}{C}$	$\frac{S}{C} + (\gamma + 1) \frac{S}{C}$	$\frac{S}{C} + (\gamma + 1) \frac{S}{C}$	$3 \frac{S}{C}$
FPDT	$\frac{S}{C \cdot \pi}$	$\frac{S}{C \cdot \pi} + (\gamma + 1) \frac{S}{C \cdot \pi}$	$(2\gamma + 1) \frac{S}{C \cdot \pi}$	$2 \frac{S}{C \cdot \pi}$
Untied Ulysses	$\frac{S}{C}$	$2 \frac{S}{C} + (\gamma + 1) \frac{S}{C \cdot \nu}$	$2 \frac{S}{C} + \gamma \frac{S}{C \cdot \nu}$	$\frac{S}{C} + 2 \frac{S}{C \cdot \nu}$

the intermediate tensors only one tile at a time. Tiled loss kernels are available in libraries such as Liger-Kernel (Hsu et al., 2025), which we leverage in our experiments. To deal with the memory usage of the feedforward phase, we adopt a similar approach to ALST by using a tiled MLP function. Furthermore, we also use tiling for RMSNorm, since we found that to be more memory-efficient compared to using `torch.compile` on the RMSNorm module. Notably, we find that Rotary Positional Encoding (Su et al., 2023) also incurs a memory overhead due to `fp32` casting, which is why we use the fused RoPE implementation from the Flash Attention API which performs in-place operations to avoid huge memory spikes. Similarly to other prior works and libraries like Unsloth (Han et al., 2023), we manage the activation memory across layers via full activation checkpointing with CPU offloading. Finally, for the attention phase, we propose **UPipe**, as described in Section 3.3.

Table 2 provides the memory consumption of different stages of the attention layer during the forward pass. In grouped-query attention, the size of key (K) and value (V) tensors is reduced by a factor of g (the GQA ratio, $g = H/G$). We define $\gamma = 1 + \frac{2}{g}$ as the combined size of Q, K, V (relative to S/C), and $\beta = 4 + \frac{4}{g}$ as the combined size of the eight tensors required for the backward pass of the attention ($Q, K, V, \text{Out}, d\text{Out}, dQ, dK, dV$). The constant factor of hidden size is omitted in the calculations for brevity. Table 6 presents a similar breakdown for the backward pass of an attention layer.

3. Untied Ulysses

As discussed above, the majority of activation tensors during training that contribute to peak memory usage can be tiled, recomputed or offloaded. In this section, we outline the design of UPipe, highlighting the key ideas that allow it to break the memory wall faced by current state-of-the-art methods in the attention stage. Moreover, our technique is more performant than prior methods when training on multi-million token sequences. Since our method builds on top of DeepSpeed-Ulysses (Jacobs et al., 2023), we will first elaborate on the mechanics of this algorithm, highlighting the opportunity for memory optimization.

3.1. DeepSpeed-Ulysses

DeepSpeed-Ulysses (DS-Ulysses) is a context parallelism technique that allows training of LLMs in a distributed setup, particularly for long-context data. The technique works by uniformly sharding a sequence of length S across C devices, so that every device has a sequence of length S/C . For a Transformer-based model, token-wise operations (feed-forward layer, RMSNorm, cross-entropy) can be applied to every sequence shard without communication. However, the attention layer requires access to the entire sequence, so it cannot be executed independently on each shard. Ulysses solves this problem by rearranging the shards: afterwards, the memory occupied by the shards is the same as before, but now every device has access to the full sequence.

Let us walk through how DeepSpeed-Ulysses works using an example from Figure 3a with $C = 2$ devices. Initially, the sequence X of size $[S, d_{model}]$ is sharded on two devices: X_0 and X_1 with size $[\frac{S}{2}, d_{model}]$ each. These shards then undergo the QKV projection to produce the query, key and value tensors. In this example, let us consider the number of heads $H = 4$, which means the query, key and value tensors have 4 heads: H_0, H_1, H_2, H_3 with $d_{head} = d_{model}/4$. Hence, the size of these tensors is $[\frac{S}{2}, 4, d_{head}]$.

Next, DS-Ulysses performs an all-to-all operation **inp_all_to_all** on the QKV tensors to *reshard* them: switching the sharding from the sequence length dimension to the head dimension. Thus, QKV tensors are resharded from $[\frac{S}{2}, 4, d_{head}]$ to $[S, 2, d_{head}]$. As a result, device 0 now has access to the full sequence for heads H_0, H_1 , while device 1 has access to the full sequence for heads H_2 and H_3 . After attention, device 0 computes outputs for heads H_0, H_1 (and device 1 computes outputs for H_2 and H_3), which are then sharded back to the original shape. Therefore, another all-to-all operation **out_all_to_all** is performed, so that the final outputs O_0 and O_1 are of shape $[\frac{S}{2}, d_{model}]$ each.

Because of all-to-all communication, DS-Ulysses has a constant communication volume with respect to the number of devices, which makes it more scalable than Ring Attention. However, it faces a memory bottleneck for long-context training, because the overhead from the communication buffers can grow to become significant.

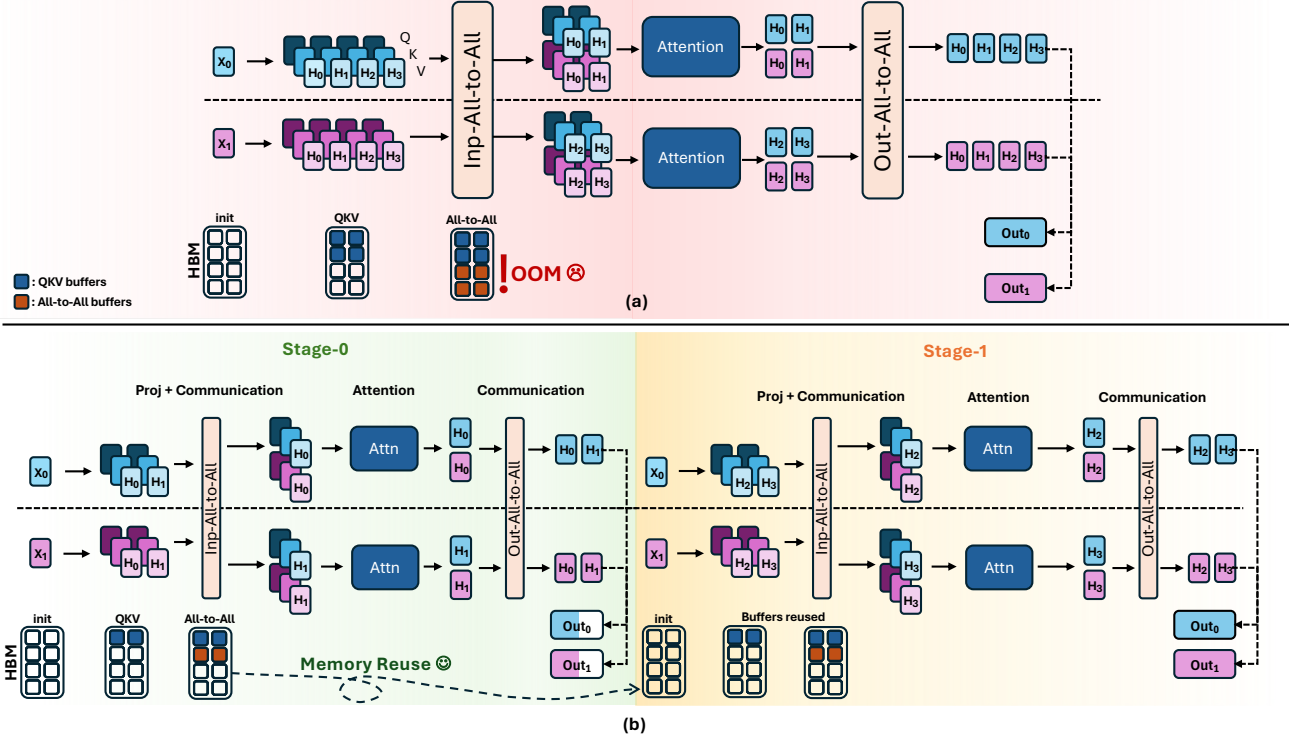


Figure 3. Illustration of (a) DeepSpeed-Ulysses and (b) UPipe designs. UPipe processes attention in a headwise *untied* manner, so that in each stage, attention is performed only on a subset of heads. This allows memory reuse across different stages, significantly reducing the peak memory usage due to attention activations. HBM (High-Bandwidth Memory) usage illustrates memory utilization due to the intermediate buffers and omits other components for brevity.

3.2. Memory Usage

The memory usage peak in DeepSpeed-Ulysses occurs during the **inp_all_to_all** operation because of the memory buffers for query, key, and value tensors and similarly sized all-to-all buffers. From Table 1, we can see that the memory usage due to these intermediate tensors is proportional to H . Our key insight is that *for long sequences and large enough models, a subset of heads is enough to reach the compute-bound regime*. Hence, we process only U heads at a time ($U < H$) so that after the input all-to-all, each device has U/C heads. Because the memory usage of intermediate tensors is proportional to the number of heads, the memory overhead reduces from $\mathcal{O}(H)$ to $\mathcal{O}(U)$. As we show later, changing U allows for a natural runtime-memory tradeoff.

3.3. Untied Ulysses: UPipe

The biggest memory overhead in DS-Ulysses comes from storing the *full-head* (i.e., all heads) QKV tensors, along with the additional *full-head* all-to-all buffers. UPipe addresses this by untying the entire attention execution in an end-to-end manner. We propose a headwise chunking scheme for performing attention, which processes only a subset of heads at a time, reducing the peak activation memory. To realize the memory benefits in practice, we also pro-

pose a GQA-scheduling technique which processes attention heads out-of-order and prevents redundant communication.

Formally, given a model with attention heads H and number of context parallel devices C , UPipe chunks the attention execution into H/U stages, processing U heads per stage. During forward pass, the execution begins by projecting the input X into Q_V^0, K_V^0 , and V_V^0 i.e., the first U heads. This is followed by **inp_all_to_all**, resulting in U/C heads per device. Note that U must be divisible by C to ensure that each device processes an integer number of heads. In the next stage, we process the next U heads while reusing the memory buffers from the previous stage (i.e., use Q_V^0 buffers to store Q_V^1 and similarly for other tensors). Therefore, the memory usage remains $\mathcal{O}(U)$ throughout the execution.

Let us now walk through the example in Figure 3b. With $H = 4, U = 2$, and $C = 2$. UPipe performs attention over $H/U = 2$ stages: processing 2 heads per stage.

Consider the execution on **Device 0**: in stage 0, the input X_0 is projected into the first two heads H_0, H_1 of QKV. Next, **inp_all_to_all** is performed on H_0, H_1 so that device 0 has H_0 for the entire sequence. Notice that during all-to-all, we only need buffers for 2 heads (as opposed to 4 heads in DS-Ulysses). We then perform attention on H_0 ,

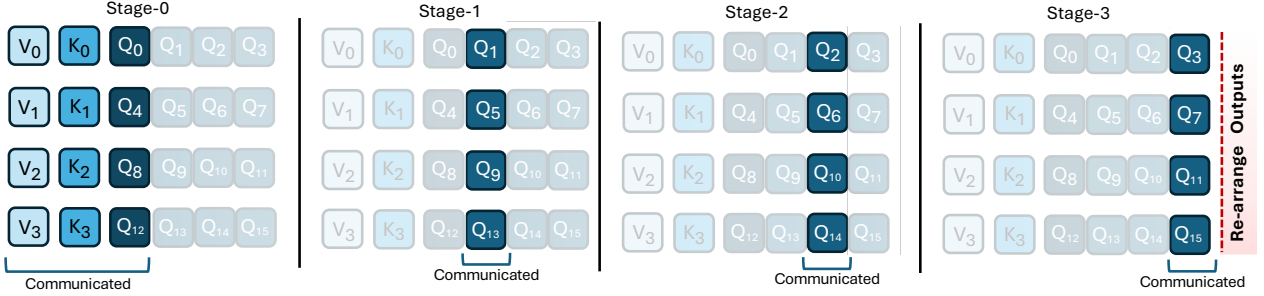


Figure 4. Illustration of UPipe’s GQA scheduling algorithm. We communicate as many unique key/value heads as possible along with the corresponding queries in stage-0. In the subsequent stages, we only communicate the next queries of the corresponding groups, reusing the key/value tensors from stage-0 until stage- G , where G is the group size.

generate output for head 0, and perform **out_all_to_all**. In the second stage, X_0 is projected into the next two heads H_2, H_3 . At this point, heads H_0, H_1 are already processed so we reuse their HBM buffers to store H_2, H_3 . Next, we perform all-to-all and similarly reuse the all-to-all buffers from stage-0. For the final output, we initialize the buffers in the beginning and fill them during execution. This avoids the concatenation of individual chunks, which otherwise degrades performance.

3.4. Memory Savings

For H heads and C devices used for context parallelism, DS-Ulysses has a total memory usage of: $6 \cdot \frac{S}{C} \cdot H \cdot d_{head}$ bytes for the QKV tensors and the same number of bytes for the all-to-all communication buffers, resulting in a total of $12 \cdot \frac{S}{C} \cdot H \cdot d_{head}$ bytes of intermediate tensors.

In case of UPipe, we can replace H with U , because a single stage processes U heads. Thus, the memory usage is $12 \cdot \frac{S}{C} \cdot U \cdot d_{head}$ bytes. To maximize memory savings, we want U to be as small as possible, and the smallest valid value is $U = C$. In this setting, the maximum memory usage of UPipe during the attention stage becomes $12 \cdot S \cdot d_{head}$. Thus, when $U = C$, the peak activation memory usage of our method is independent of the number of heads.

Taking Qwen3-32B as an example with $H = 64$ and using a single $8 \times H100$ node (i.e., $C = 8$), DS-Ulysses requires $96 \cdot S \cdot d_{head}$. By contrast, UPipe requires $12 \cdot S \cdot d_{head}$, lowering the memory usage of intermediate activations for self-attention by **87.5%**.

4. Implementation

We use TorchTitan (Liang et al., 2025) as the training framework to integrate the implementation of UPipe, due to its flexibility and performance. We use the same framework for Unified Sequence Parallelism (USP) baselines to ensure fair comparison with respect to the training setup. For the core Transformer functionality, we override the attention

module with our implementation, and we replace FeedForward (FFN), RMSNorm and CELoss modules with publicly available optimized implementations (ALST, Liger-Kernel).

We integrate the core transformer modules inside TorchTitan via simple drop-in replacement of the existing modules. We use the hybrid attention implementation from USP as the baselines for Ulysses and Ring Attention, which includes a load balanced zig-zag Ring Attention implementation. UPipe uses the same code structure as USP, so it can be easily extended for a hybrid (Ulysses+Ring) setup. For all-to-all communication, we use the non-QKVPacked variant from USP, which communicates queries, keys, and values sequentially to avoid memory overhead from simultaneous communication.

For operations independent along the sequence length, such as FFN and RMSNorm, we use TiledCompute, a tiling mechanism introduced by ALST. To determine the tile size, we use the same method as the authors of ALST by using a square tile of size $[d_{model} \times d_{model}]$. We use FusedLinearCrossEntropyLoss from Liger-Kernel for memory-efficient loss computation. This kernel fuses the final linear projection with the cross-entropy loss, computing logits and loss in a tiled manner to avoid materializing the full fp32 logits tensor in memory.

4.1. GQA Scheduling

Because of its memory benefits, Grouped Query Attention (GQA, Ainslie et al., 2023) is an important architectural component of modern Transformer models (Grattafiori et al., 2024; Jiang et al., 2023; Yang et al., 2025). To ensure the GQA benefits are retained, we make our design GQA-compatible. This requires rearranging the query tensors to reuse the KV tensors communicated in the previous stage.

Assuming $U = C$, recall that UPipe processes C heads per stage, so that after all-to-all, every device performs attention on a single head. For a GQA model with group size G , only C/G of the first C heads are unique. For example,

consider $C = 4$ and $G = 4$. With naive processing, stage-0 would process query heads Q_0, Q_1, Q_2, Q_3 with the corresponding key heads K_0, K_0, K_0, K_0 . Since each device communicates $C - 1$ query, key and value heads per stage, the total communication volume across H/C stages is $\mathcal{O}(3 \cdot \frac{H}{C} \cdot C - 1)$.

Referring to Figure 4, one might observe that we could communicate K_0, K_1, K_2, K_3 (i.e., all the unique key tensors) in stage 0. We would then need to send the corresponding query tensors (i.e., Q_0, Q_4, Q_8, Q_{12}). However, in the next stage, we do not need to communicate any key (or value) tensors. We can now choose the next query tensors from the groups (i.e., Q_1, Q_5, Q_9, Q_{13}), because the corresponding key (and value) tensors were already communicated in stage 0. In this case, for every G stages, we communicate $C - 1$ query, key and value heads in the first stage, and only $C - 1$ query heads in the subsequent stages. Thus, the total communication volume is $\mathcal{O}((3 + G - 1) \cdot \frac{H}{C \cdot G} \cdot C - 1)$ which is always less than the naive processing (since $G > 1$).

5. Experiments

We now present the experimental results using UPipe, comparing it with multiple SOTA baselines, as well as standard context parallelism approaches. We run the experiments on two different model families across multiple context lengths, comparing the maximum context length supported by different techniques and their throughput in each setup. For all experiments with UPipe, we set the chunk size to be the same as the number of context-parallel devices ($U = C$), to demonstrate the highest memory efficiency.

5.1. Setup

System Specifications: We run our experiments on NVIDIA $8 \times H100$ nodes with 80GiB of HBM3 on-chip DRAM per GPU, connected via 4th generation NVLink with 900GBps bidirectional bandwidth for intra-node communication, and Mellanox Infiniband with 400 Gbps bidirectional bandwidth for inter-node communication. We use a 64-core Intel x86 CPU per node with 1.9TiB RAM.

Models: We use Llama3-8B (Grattafiori et al., 2024) and Qwen3-32B (Yang et al., 2025) models to run our experiments. Llama3-8B has $H = 32$ query heads (and 8 key-value heads), thus allowing UPipe to process attention in $H/C = 4$ stages. Qwen3-32B has 64 query heads (and 8 key-value heads), so UPipe processes it in 8 stages. Note that we use $C = 8$ here, because we always restrict Ulysses context parallelism degree to 8 and use rest for ring (in a USP-Hybrid style setup as discussed in 5.2.1).

Framework: We use TorchTitan as the distributed training framework, and Flash Attention-3 (FA3) (Shah et al., 2024) for all the experiments. Note that FPDT does not natively

support FA3, so we patched their implementation with FA3 support for a fair comparison against UPipe.

Distributed Setup: We use context parallelism over $8 \times H100$ s for our training. We use PyTorch’s Fully Sharded Data Parallel (Zhao et al., 2023) to distribute the parameters, gradients and optimizer states across all the GPUs.

For efficient management of activation memory, we use full activation-checkpointing with CPU offloading, to maintain consistency with FPDT. For all sequence lengths except 5M, we allow the CPU offloaded activations to reside on the non-swappable CPU RAM by setting `PIN_MEMORY` to `True`. For 5M, we set this to `False` due to the CPU RAM constraints (1.9TB). For better memory management, we set `PYTORCH_CUDA_ALLOC_CONF=expandable_segments:True` similar to ALST.

5.2. Baselines

We compare UPipe’s performance and memory efficiency against multiple baselines. Fully Pipelined Distributed Transformer (FPDT) is a long-context training recipe which processes attention by chunking along the sequence length dimension and using online softmax to perform full attention. It mitigates the prohibitive memory requirements by asynchronously offloading chunks to CPU, keeping only the necessary chunks on GPU, and using double buffer mechanism to overlap communication with computation. It can support a maximum sequence of 4M tokens when training Llama3-8B on a single $8 \times H100$. For standard Ulysses and Ring attention baselines, we use USP implementation, as it provides an easy-to-use interface for modifications. Additionally, we also compare against the ring implementation in native PyTorch. We omit Arctic Long Sequence Training (ALST) in our experiments because our modified version of USP-Ulysses (which uses DS-Ulysses, offloaded activation checkpointing, and tiling for MLP / CELoss) resembles with the ALST design. Moreover, unlike ALST, we do not offload optimizer states onto the CPU in any of the experiments to avoid throughput degradation.

5.2.1. MULTI-NODE TRAINING

For multi-node experiments, we use a similar setup as USP-Hybrid, using *8-ulysses-2-ring*, that is, Ulysses over 8 GPUs within the node, and Ring across 2 nodes. This is a common setup for hybrid context parallelism (e.g. Team Wan et al., 2025) to allow faster all-to-all for Ulysses within the node, and slower ring communication across nodes. Note that FPDT does not support hybrid sequence parallelism, so we use the standard *16-ulysses-1-ring* setup.

We also compare against ring-only baselines: USP-Ring and native PyTorch ring. Both these baselines use zigzag load balancing, ensuring fair work distribution across all ranks.

Table 3. **Throughput comparison** (Tokens/second/GPU) for **Llama3-8B** (8×H100s) and **Qwen3-32B** (16×H100s) across varying sequence lengths. By reducing the peak memory usage and eliminating CUDA allocation retries, our approach achieves the highest throughput for sequence lengths ≥ 2 M. Notably, on a single 8×H100 node, our method scales Llama3-8B to a 5M-token sequence length—a 25% improvement over the previous state-of-the-art. **OOM**: Out of Memory. **Note**: FPDT execution fails at lengths > 4 M.

	Model	128K	256K	512K	1M	2M	3M	4M	5M
Llama3-8B	Native PyTorch	1373.87	845.99	474.30	249.85	OOM	–	–	–
	Ring	2064.90	1387.67	841.05	458.51	237.99	159.96	OOM	–
	Ulysses	2320.47	1503.80	878.63	475.33	246.05	162.41	OOM	–
	FPDT	1171.68	884.75	621.20	382.42	219.53	153.48	119.76	–
	UPipe	2281.05	1487.29	867.17	472.53	246.07	166.32	125.56	98.25
Qwen3-32B	Native PyTorch	127.03	112.20	91.39	OOM	–	–	–	–
	Ring	418.39	308.88	194.44	110.27	58.45	OOM	–	–
	Ulysses	545.29	370.70	217.04	117.02	59.98	OOM	–	–
	FPDT	286.40	217.85	151.91	95.88	55.41	38.86	27.66	–
	UPipe	483.29	339.56	204.46	113.26	59.56	40.42	29.97	OOM

5.3. Performance

5.3.1. SINGLE-NODE TRAINING

Llama3-8B: Table 3 (top) reports single-node throughput (tokens/second/GPU) for Llama3-8B across increasing sequence lengths. Ulysses delivers strong throughput by using a single all-to-all per attention, but its full-head QKV and communication buffers make activation memory the primary limiter at multi-million-token contexts. FPDT can push context length further by tiling attention and offloading to CPU, but it pays a substantial throughput penalty from frequent CPU–GPU transfers. UPipe bridges this gap: at shorter sequences it is slightly slower than Ulysses due to additional stage launches, but this overhead is amortized as context grows (as shown in Table 5). At longer sequences (≥ 2 M), UPipe matches Ulysses throughput while using much lower GPU memory, enabling training at 5M tokens on a single 8×H100 node. In effect, UPipe preserves the throughput of Ulysses while delivering memory efficiency closer to offloading-based approaches, improving the maximum single-node context length over FPDT (4M) by **25%**.

5.3.2. MULTI-NODE TRAINING

Llama3-8B: Figure 5 shows the comparison of UPipe and USP-Hybrid on a 16×H100 setup. UPipe is more memory efficient than USP-Hybrid at all sequence lengths from 512K to 6M tokens, and supports context lengths upto 8M tokens, improving upon USP-Hybrid by **33%**. The throughput of UPipe is comparable to USP-Hybrid at all sequence lengths, highlighting UPipe’s runtime efficiency.

Qwen3-32B: Table 3 (bottom) summarizes the throughput comparison of different methods when training Qwen3-32B on a 16×H100 setup. UPipe outperforms all other methods

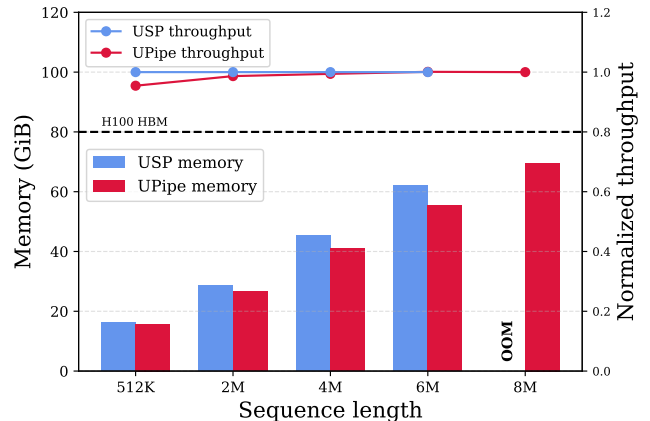


Figure 5. **Llama3-8B:** Peak GPU memory usage and throughput (normalized w.r.t USP-Hybrid) comparison of UPipe and USP-Hybrid at different sequence lengths on 16×H100s. Our method significantly outperforms USP-Hybrid in terms of memory efficiency, and allows a maximum context size of **8M**, improving upon USP-Hybrid (6M tokens) by **33%**, while maintaining throughput.

for sequences ≥ 2 M. Notably, UPipe always outperforms FPDT across all sequence lengths in terms of throughput. In terms of maximum sequence length, our method can support 4M token sequences, $2\times$ more than Ulysses (2M tokens), while delivering **8.3%** better performance than FPDT.

Additionally, we also report the maximum allocated memory in Appendix Table 4. UPipe provides best memory efficiency compared to other methods except FPDT. However, FPDT suffers from performance degradation due to frequent CPU transfers. Nevertheless, our method should be composable with FPDT due to orthogonal chunking dimensions, allowing benefits from both the methods.

For the above experiments, our aim was to show the maximum memory efficiency of UPipe so we chose $U = C$.

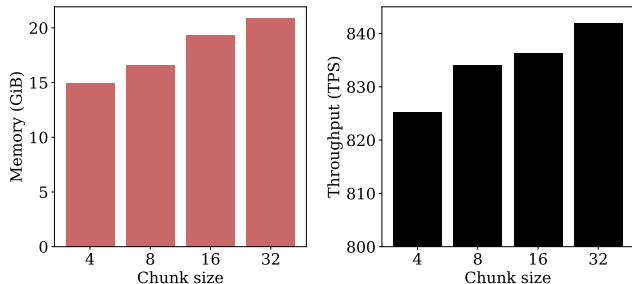


Figure 6. **Llama3-8B**: Ablation analysis of UPipe’s head-chunk size U , with 512K context size on $C = 4$ GPUs. Smaller chunk size yields better memory efficiency at the cost of throughput and vice versa, allowing a trade-off between memory and throughput.

Next, we present an ablation on U discussing the associated tradeoffs between memory and throughput.

5.4. Ablation on the head-chunk size U

As shown in Figure 6, we perform an ablation study on UPipe’s hyperparameter U i.e., the number of heads processed per stage. It allows memory-runtime tradeoff, where larger U corresponds to more heads processed per stage, resulting in higher memory usage and lower runtime. Conversely, when $U = C$, UPipe provides maximum memory benefits, at the cost of slight performance degradation due to kernel launch overhead (though at longer context lengths, this overhead is amortized by the increased length as shown in Table 5). We perform the ablation using Llama3-8B on $4 \times$ H100 GPUs, with a context size of 512K tokens.

6. Conclusion

In this paper, we introduced UPipe, an *untied* variant of Ulysses that reduces attention activation memory by chunking attention end-to-end at the head level. Our experimental evaluation demonstrates that these memory gains translate into practical context scaling without sacrificing throughput. On Llama3-8B, UPipe reaches **5M** tokens on a single $8 \times$ H100 node (**25%** beyond FPDT), and scales to **8M** tokens on $16 \times$ H100 while maintaining throughput comparable to widely deployed baselines such as DeepSpeed-Ulysses and Unified Sequence Parallelism. On larger models, UPipe reduces attention intermediate tensor memory by up to 87.5% (e.g., Qwen3-32B at $C = 8$), helping avoid allocation retries that otherwise degrades performance.

Overall, UPipe provides a practical path to pushing the context frontier: it is simple, compatible with existing context-parallel training pipelines, and delivers substantial memory efficiency improvements while preserving the throughput. We expect UPipe to serve as a useful building block for future long-context systems, especially as models and modalities continue to demand larger effective context windows.

References

- Ainslie, J., Lee-Thorp, J., de Jong, M., Zemlyanskiy, Y., Lebrón, F., and Sanghai, S. Gqa: Training generalized multi-query transformer models from multi-head checkpoints, 2023. URL <https://arxiv.org/abs/2305.13245>.
- Bekman, S., Rajbhandari, S., Wyatt, M., Rasley, J., Ruwase, T., Yao, Z., Qiao, A., and He, Y. Arctic long sequence training: Scalable and efficient training for multi-million token sequences, 2025. URL <https://arxiv.org/abs/2506.13996>.
- Chen, A., Li, A., Gong, B., Jiang, B., Fei, B., Yang, B., Shan, B., Yu, C., Wang, C., Zhu, C., et al. Minimax-m1: Scaling test-time compute efficiently with lightning attention. *arXiv preprint arXiv:2506.13585*, 2025.
- Chia, Y. K., Cheng, L., Chan, H. P., Liu, C., Song, M., Aljunied, S. M., Poria, S., and Bing, L. M-longdoc: A benchmark for multimodal super-long document understanding and a retrieval-aware tuning framework, 2024. URL <https://arxiv.org/abs/2411.06176>.
- Dao, T., Fu, D. Y., Ermon, S., Rudra, A., and Ré, C. FlashAttention: Fast and memory-efficient exact attention with IO-awareness. In *Advances in Neural Information Processing Systems (NeurIPS)*, 2022.
- Fang, J. and Zhao, S. Usp: A unified sequence parallelism approach for long context generative ai, 2024. URL <https://arxiv.org/abs/2405.07719>.
- Gemini Team. Gemini 3.0: A new era of intelligence with gemini 3. *Google DeepMind*, 2025.
- Grattafiori, A., Dubey, A., Jauhri, A., Pandey, A., Kadian, A., Al-Dahle, A., Letman, A., Mathur, A., Schelten, A., Vaughan, A., Yang, A., Fan, A., Goyal, A., Hartshorn, A., Yang, A., Mitra, A., Sravankumar, A., Korenev, A., Hinsvark, A., Rao, A., Zhang, A., Rodriguez, A., Gregerson, A., Spataru, A., Roziere, B., Biron, B., Tang, B., Chern, B., Caucheteux, C., Nayak, C., Bi, C., Marra, C., McConnell, C., Keller, C., Touret, C., Wu, C., Wong, C., Ferrer, C. C., Nikolaidis, C., Allonsius, D., Song, D., Pintz, D., Livshits, D., Wyatt, D., Esiobu, D., Choudhary, D., Mahajan, D., Garcia-Olano, D., Perino, D., Hupkes, D., Lacomkin, E., AlBadawy, E., Lobanova, E., Dinan, E., Smith, E. M., Radenovic, F., Guzmán, F., Zhang, F., Synnaeve, G., Lee, G., Anderson, G. L., Thattai, G., Nail, G., Mialon, G., Pang, G., Cucurell, G., Nguyen, H., Korevaar, H., Xu, H., Touvron, H., Zarov, I., Ibarra, I. A., Kloumann, I., Misra, I., Evtimov, I., Zhang, J., Copet, J., Lee, J., Geffert, J., Vranes, J., Park, J., Mahadeokar, J., Shah, J., van der Linde, J., Billock, J., Hong, J., Lee, J., Fu, J., Chi, J., Huang, J., Liu, J., Wang, J., Yu, J., Bitton,

- J., Spisak, J., Park, J., Rocca, J., Johnstun, J., Saxe, J., Jia, J., Alwala, K. V., Prasad, K., Upasani, K., Plawiak, K., Li, K., Heafield, K., Stone, K., El-Arini, K., Iyer, K., Malik, K., Chiu, K., Bhalla, K., Lakhota, K., Rantala-Yearly, L., van der Maaten, L., Chen, L., Tan, L., Jenkins, L., Martin, L., Madaan, L., Malo, L., Blecher, L., Landzaat, L., de Oliveira, L., Muzzi, M., Pasupuleti, M., Singh, M., Paluri, M., Kardas, M., Tsimpoukelli, M., Oldham, M., Rita, M., Pavlova, M., Kambadur, M., Lewis, M., Si, M., Singh, M. K., Hassan, M., Goyal, N., Torabi, N., Bashlykov, N., Bogoychev, N., Chatterji, N., Zhang, N., Duchenne, O., Çelebi, O., Alrassy, P., Zhang, P., Li, P., Vasic, P., Weng, P., Bhargava, P., Dubal, P., Krishnan, P., Koura, P. S., Xu, P., He, Q., Dong, Q., Srinivasan, R., Ganapathy, R., Calderer, R., Cabral, R. S., Stojnic, R., Raileanu, R., Maheswari, R., Girdhar, R., Patel, R., Sauvestre, R., Polidoro, R., Sumbaly, R., Taylor, R., Silva, R., Hou, R., Wang, R., Hosseini, S., Chennabasappa, S., Singh, S., Bell, S., Kim, S. S., Edunov, S., Nie, S., Narang, S., Raparthy, S., Shen, S., Wan, S., Bhosale, S., Zhang, S., Vandenhende, S., Batra, S., Whitman, S., Sootla, S., Collot, S., Gururangan, S., Borodinsky, S., Herman, T., Fowler, T., Sheasha, T., Georgiou, T., Scialom, T., Speckbacher, T., Mihaylov, T., Xiao, T., Karn, U., Goswami, V., Gupta, V., Ramanathan, V., Kerkez, V., Gonguet, V., Do, V., Vogeti, V., Albiero, V., Petrovic, V., Chu, W., Xiong, W., Fu, W., Meers, W., Martinet, X., Wang, X., Wang, X., Tan, X. E., Xia, X., Xie, X., Jia, X., Wang, X., Goldschlag, Y., Gaur, Y., Babaei, Y., Wen, Y., Song, Y., Zhang, Y., Li, Y., Mao, Y., Coudert, Z. D., Yan, Z., Chen, Z., Papakipos, Z., Singh, A., Srivastava, A., Jain, A., Kelsey, A., Shajnfeld, A., Gangidi, A., Victoria, A., Goldstand, A., Menon, A., Sharma, A., Boesenberg, A., Baevski, A., Feinstein, A., Kallet, A., Sangani, A., Teo, A., Yunus, A., Lupu, A., Alvarado, A., Caples, A., Gu, A., Ho, A., Poulton, A., Ryan, A., Ramchandani, A., Dong, A., Franco, A., Goyal, A., Saraf, A., Chowdhury, A., Gabriel, A., Bharambe, A., Eisenman, A., Yazdan, A., James, B., Maurer, B., Leonhardi, B., Huang, B., Loyd, B., Paola, B. D., Paranjape, B., Liu, B., Wu, B., Ni, B., Hancock, B., Wasti, B., Spence, B., Stojkovic, B., Gamido, B., Montalvo, B., Parker, C., Burton, C., Mejia, C., Liu, C., Wang, C., Kim, C., Zhou, C., Hu, C., Chu, C.-H., Cai, C., Tindal, C., Feichtenhofer, C., Gao, C., Civin, D., Beaty, D., Kreymer, D., Li, D., Adkins, D., Xu, D., Testuggine, D., David, D., Parikh, D., Liskovich, D., Foss, D., Wang, D., Le, D., Holland, D., Dowling, E., Jamil, E., Montgomery, E., Presani, E., Hahn, E., Wood, E., Le, E.-T., Brinkman, E., Arcaute, E., Dunbar, E., Smothers, E., Sun, F., Kreuk, F., Tian, F., Kokkinos, F., Ozgenel, F., Caggioni, F., Kanayet, F., Seide, F., Florez, G. M., Schwarz, G., Badeer, G., Swee, G., Halpern, G., Herman, G., Sizov, G., Guangyi, Zhang, Lakshminarayanan, G., Inan, H., Shojanazeri, H., Zou, H., Wang, H., Zha, H., Habeeb, H., Rudolph, H., Suk, H., Aspegren, H., Goldman, H., Zhan, H., Damaj, I., Molybog, I., Tufanov, I., Leontiadis, I., Veliche, I.-E., Gat, I., Weissman, J., Geboski, J., Kohli, J., Lam, J., Asher, J., Gaya, J.-B., Marcus, J., Tang, J., Chan, J., Zhen, J., Reizenstein, J., Teboul, J., Zhong, J., Jin, J., Yang, J., Cummings, J., Carvill, J., Shepard, J., McPhie, J., Torres, J., Ginsburg, J., Wang, J., Wu, K., U, K. H., Saxena, K., Khandelwal, K., Zand, K., Matosich, K., Veeraraghavan, K., Michelena, K., Li, K., Jagadeesh, K., Huang, K., Chawla, K., Huang, K., Chen, L., Garg, L., A, L., Silva, L., Bell, L., Zhang, L., Guo, L., Yu, L., Moshkovich, L., Wehrstedt, L., Khabsa, M., Avalani, M., Bhatt, M., Mankus, M., Hasson, M., Lennie, M., Reso, M., Groshev, M., Naumov, M., Lathi, M., Keneally, M., Liu, M., Seltzer, M. L., Valko, M., Restrepo, M., Patel, M., Vyatskov, M., Samvelyan, M., Clark, M., Macey, M., Wang, M., Hermoso, M. J., Metanat, M., Rastegari, M., Bansal, M., Santhanam, N., Parks, N., White, N., Bawa, N., Singhal, N., Egebo, N., Usunier, N., Mehta, N., Laptev, N. P., Dong, N., Cheng, N., Chernoguz, O., Hart, O., Salpekar, O., Kalinli, O., Kent, P., Parekh, P., Saab, P., Balaji, P., Rittner, P., Bontrager, P., Roux, P., Dollar, P., Zvyagina, P., Ratanchandani, P., Yuvraj, P., Liang, Q., Alao, R., Rodriguez, R., Ayub, R., Murthy, R., Nayani, R., Mitra, R., Parthasarathy, R., Li, R., Hogan, R., Battey, R., Wang, R., Howes, R., Rinott, R., Mehta, S., Siby, S., Bondu, S. J., Datta, S., Chugh, S., Hunt, S., Dhillon, S., Sidorov, S., Pan, S., Mahajan, S., Verma, S., Yamamoto, S., Ramaswamy, S., Lindsay, S., Lindsay, S., Feng, S., Lin, S., Zha, S. C., Patil, S., Shankar, S., Zhang, S., Zhang, S., Wang, S., Agarwal, S., Sajuyigbe, S., Chintala, S., Max, S., Chen, S., Kehoe, S., Satterfield, S., Govindaprasad, S., Gupta, S., Deng, S., Cho, S., Virk, S., Subramanian, S., Choudhury, S., Goldman, S., Remez, T., Glaser, T., Best, T., Koehler, T., Robinson, T., Li, T., Zhang, T., Matthews, T., Chou, T., Shaked, T., Vontimitta, V., Ajayi, V., Montanez, V., Mohan, V., Kumar, V. S., Mangla, V., Ionescu, V., Poenaru, V., Mihailescu, V. T., Ivanov, V., Li, W., Wang, W., Jiang, W., Bouaziz, W., Constable, W., Tang, X., Wu, X., Wang, X., Wu, X., Gao, X., Kleinman, Y., Chen, Y., Hu, Y., Jia, Y., Qi, Y., Li, Y., Zhang, Y., Zhang, Y., Adi, Y., Nam, Y., Yu, Wang, Zhao, Y., Hao, Y., Qian, Y., Li, Y., He, Y., Rait, Z., DeVito, Z., Rosnbrick, Z., Wen, Z., Yang, Z., Zhao, Z., and Ma, Z. The llama 3 herd of models, 2024. URL <https://arxiv.org/abs/2407.21783>.
- Han, D., Han, M., and team, U. Unslloth, 2023. URL <https://github.com/unsllothai/unslloth>.
- Hori, T., Moritz, N., Hori, C., and Roux, J. L. Advanced long-context end-to-end speech recognition using context-expanded transformers. *ArXiv*, abs/2104.09426, 2021. URL <https://api.semanticscholar.org/CorpusID:233296591>.

- Hsu, P.-L., Dai, Y., Kothapalli, V., Song, Q., Tang, S., Zhu, S., Shimizu, S., Sahni, S., Ning, H., Chen, Y., and Wang, Z. Liger-kernel: Efficient triton kernels for LLM training. In *Championing Open-source DEvelopment in ML Workshop @ ICML25*, 2025. URL <https://openreview.net/forum?id=36SjAIT42G>.
- Hui, B., Yang, J., Cui, Z., Yang, J., Liu, D., Zhang, L., Liu, T., Zhang, J., Yu, B., Lu, K., Dang, K., Fan, Y., Zhang, Y., Yang, A., Men, R., Huang, F., Zheng, B., Miao, Y., Quan, S., Feng, Y., Ren, X., Ren, X., Zhou, J., and Lin, J. Qwen2.5-coder technical report, 2024. URL <https://arxiv.org/abs/2409.12186>.
- Jacobs, S. A., Tanaka, M., Zhang, C., Zhang, M., Song, S. L., Rajbhandari, S., and He, Y. DeepSpeed ulysses: System optimizations for enabling training of extreme long sequence transformer models, 2023. URL <https://arxiv.org/abs/2309.14509>.
- Jiang, A. Q., Sablayrolles, A., Mensch, A., Bamford, C., Chaplot, D. S., de las Casas, D., Bressand, F., Lengyel, G., Lample, G., Saulnier, L., Lavaud, L. R., Lachaux, M.-A., Stock, P., Scao, T. L., Lavril, T., Wang, T., Lacroix, T., and Sayed, W. E. Mistral 7b, 2023. URL <https://arxiv.org/abs/2310.06825>.
- Jiang, Z., Ma, X., and Chen, W. Longrag: Enhancing retrieval-augmented generation with long-context llms, 2024. URL <https://arxiv.org/abs/2406.15319>.
- Kimi Team, Bai, Y., Bao, Y., Chen, G., Chen, J., Chen, N., Chen, R., Chen, Y., Chen, Y., Chen, Y., Chen, Z., Cui, J., Ding, H., Dong, M., Du, A., Du, C., Du, D., Du, Y., Fan, Y., Feng, Y., Fu, K., Gao, B., Gao, H., Gao, P., Gao, T., Gu, X., Guan, L., Guo, H., Guo, J., Hu, H., Hao, X., He, T., He, W., He, W., Hong, C., Hu, Y., Hu, Z., Huang, W., Huang, Z., Huang, Z., Jiang, T., Jiang, Z., Jin, X., Kang, Y., Lai, G., Li, C., Li, F., Li, H., Li, M., Li, W., Li, Y., Li, Y., Li, Z., Li, Z., Lin, H., Lin, X., Lin, Z., Liu, C., Liu, C., Liu, H., Liu, J., Liu, J., Liu, L., Liu, S., Liu, T. Y., Liu, T., Liu, W., Liu, Y., Liu, Y., Liu, Y., Liu, Y., Liu, Z., Lu, E., Lu, L., Ma, S., Ma, X., Ma, Y., Mao, S., Mei, J., Men, X., Miao, Y., Pan, S., Peng, Y., Qin, R., Qu, B., Shang, Z., Shi, L., Shi, S., Song, F., Su, J., Su, Z., Sun, X., Sung, F., Tang, H., Tao, J., Teng, Q., Wang, C., Wang, D., Wang, F., Wang, H., Wang, J., Wang, J., Wang, J., Wang, S., Wang, S., Wang, Y., Wang, Y., Wang, Y., Wang, Y., Wang, Y., Wang, Z., Wang, Z., Wang, Z., Wei, C., Wei, Q., Wu, W., Wu, X., Wu, Y., Xiao, C., Xie, X., Xiong, W., Xu, B., Xu, J., Xu, J., Xu, L. H., Xu, L., Xu, S., Xu, W., Xu, X., Xu, Y., Xu, Z., Yan, J., Yan, Y., Yang, X., Yang, Y., Yang, Z., Yang, Z., Yang, Z., Yao, H., Yao, X., Ye, W., Ye, Z., Yin, B., Yu, L., Yuan, E., Yuan, H., Yuan, M., Zhan, H., Zhang, D., Zhang, H., Zhang, W., Zhang, X., Zhang, Y., Zhang, Y., Zhang, Y., Zhang, Y., Zhang, Y., Zhang, Y., Zhang, Z., Zhao, H., Zhao, Y., Zheng, H., Zheng, S., Zhou, J., Zhou, X., Zhou, Z., Zhu, Z., Zhuang, W., and Zu, X. Kimi k2: Open agentic intelligence, 2025. URL <https://arxiv.org/abs/2507.20534>.
- Korthikanti, V., Casper, J., Lym, S., McAfee, L., Andersch, M., Shoeybi, M., and Catanzaro, B. Reducing activation recomputation in large transformer models, 2022. URL <https://arxiv.org/abs/2205.05198>.
- Li, R., Allal, L. B., Zi, Y., Muennighoff, N., Kocetkov, D., Mou, C., Marone, M., Akiki, C., Li, J., Chim, J., Liu, Q., Zheltonozhskii, E., Zhuo, T. Y., Wang, T., Dehaene, O., Davaadorj, M., Lamy-Poirier, J., Monteiro, J., Shliazhko, O., Gontier, N., Meade, N., Zebaze, A., Yee, M.-H., Umapathi, L. K., Zhu, J., Lipkin, B., Oblokulov, M., Wang, Z., Murthy, R., Stillerman, J., Patel, S. S., Abulkhanov, D., Zocca, M., Dey, M., Zhang, Z., Fahmy, N., Bhattacharyya, U., Yu, W., Singh, S., Luccioni, S., Villegas, P., Kunakov, M., Zhdanov, F., Romero, M., Lee, T., Timor, N., Ding, J., Schlesinger, C., Schoelkopf, H., Ebert, J., Dao, T., Mishra, M., Gu, A., Robinson, J., Anderson, C. J., Dolan-Gavitt, B., Contractor, D., Reddy, S., Fried, D., Bahdanau, D., Jernite, Y., Ferrandis, C. M., Hughes, S., Wolf, T., Guha, A., von Werra, L., and de Vries, H. Starcoder: may the source be with you!, 2023a. URL <https://arxiv.org/abs/2305.06161>.
- Li, S., Xue, F., Baranwal, C., Li, Y., and You, Y. Sequence parallelism: Long sequence training from system perspective, 2022. URL <https://arxiv.org/abs/2105.13120>.
- Li, S., Xue, F., Baranwal, C., Li, Y., and You, Y. Sequence parallelism: Long sequence training from system perspective. In Rogers, A., Boyd-Graber, J., and Okazaki, N. (eds.), *Proceedings of the 61st Annual Meeting of the Association for Computational Linguistics (Volume 1: Long Papers)*, pp. 2391–2404, Toronto, Canada, July 2023b. Association for Computational Linguistics. doi: 10.18653/v1/2023.acl-long.134. URL <https://aclanthology.org/2023.acl-long.134/>.
- Liang, W., Liu, T., Wright, L., Constable, W., Gu, A., Huang, C.-C., Zhang, I., Feng, W., Huang, H., Wang, J., Purandare, S., Nadathur, G., and Idreos, S. TorchTitan: One-stop pytorch native solution for production ready LLM pretraining. In *The Thirteenth International Conference on Learning Representations*, 2025. URL <https://openreview.net/forum?id=SFN6Wm7YBI>.
- Liu, H., Zaharia, M., and Abbeel, P. Ring attention with blockwise transformers for near-infinite context, 2023. URL <https://arxiv.org/abs/2310.01889>.

- Sand.ai, Teng, H., Jia, H., Sun, L., Li, L., Li, M., Tang, M., Han, S., Zhang, T., Zhang, W. Q., Luo, W., Kang, X., Sun, Y., Cao, Y., Huang, Y., Lin, Y., Fang, Y., Tao, Z., Zhang, Z., Wang, Z., Liu, Z., Shi, D., Su, G., Sun, H., Pan, H., Wang, J., Sheng, J., Cui, M., Hu, M., Yan, M., Yin, S., Zhang, S., Liu, T., Yin, X., Yang, X., Song, X., Hu, X., Zhang, Y., and Li, Y. Magi-1: Autoregressive video generation at scale, 2025. URL <https://arxiv.org/abs/2505.13211>.
- Shah, J., Bikshandi, G., Zhang, Y., Thakkar, V., Ramani, P., and Dao, T. Flashattention-3: Fast and accurate attention with asynchrony and low-precision, 2024. URL <https://arxiv.org/abs/2407.08608>.
- Su, J., Lu, Y., Pan, S., Murtadha, A., Wen, B., and Liu, Y. Roformer: Enhanced transformer with rotary position embedding, 2023. URL <https://arxiv.org/abs/2104.09864>.
- Team Wan, Wang, A., Ai, B., Wen, B., Mao, C., Xie, C.-W., Chen, D., Yu, F., Zhao, H., Yang, J., Zeng, J., Wang, J., Zhang, J., Zhou, J., Wang, J., Chen, J., Zhu, K., Zhao, K., Yan, K., Huang, L., Feng, M., Zhang, N., Li, P., Wu, P., Chu, R., Feng, R., Zhang, S., Sun, S., Fang, T., Wang, T., Gui, T., Weng, T., Shen, T., Lin, W., Wang, W., Wang, W., Zhou, W., Wang, W., Shen, W., Yu, W., Shi, X., Huang, X., Xu, X., Kou, Y., Lv, Y., Li, Y., Liu, Y., Wang, Y., Zhang, Y., Huang, Y., Li, Y., Wu, Y., Liu, Y., Pan, Y., Zheng, Y., Hong, Y., Shi, Y., Feng, Y., Jiang, Z., Han, Z., Wu, Z.-F., and Liu, Z. Wan: Open and advanced large-scale video generative models, 2025. URL <https://arxiv.org/abs/2503.20314>.
- Vaswani, A., Shazeer, N., Parmar, N., Uszkoreit, J., Jones, L., Gomez, A. N., Kaiser, L., and Polosukhin, I. Attention is all you need. In *Advances in Neural Information Processing Systems (NeurIPS)*, 2017.
- Wu, B., Zou, C., Li, C., Huang, D., Yang, F., Tan, H., Peng, J., Wu, J., Xiong, J., Jiang, J., Linus, Patrol, Zhang, P., Chen, P., Zhao, P., Tian, Q., Liu, S., Kong, W., Wang, W., He, X., Li, X., Deng, X., Zhe, X., Li, Y., Long, Y., Peng, Y., Wu, Y., Liu, Y., Wang, Z., Dai, Z., Peng, B., Li, C., Gong, G., Xiao, G., Tian, J., Lin, J., Liu, J., Zhang, J., Lian, J., Pan, K., Wang, L., Niu, L., Chen, M., Chen, M., Zheng, M., Yang, M., Hu, Q., Yang, Q., Xiao, Q., Wu, R., Xu, R., Yuan, R., Sang, S., Huang, S., Gong, S., Huang, S., Guo, W., Yuan, X., Chen, X., Hu, X., Sun, W., Wu, X., Ren, X., Yuan, X., Mi, X., Zhang, Y., Sun, Y., Lu, Y., Li, Y., Huang, Y., Tang, Y., Li, Y., Deng, Y., Zhou, Y., Hu, Z., Liu, Z., Yang, Z., Yang, Z., Lu, Z., Zhou, Z., and Zhong, Z. Hunyuanvideo 1.5 technical report, 2025. URL <https://arxiv.org/abs/2511.18870>.
- Yang, A., Li, A., Yang, B., Zhang, B., Hui, B., Zheng, B., Yu, B., Gao, C., Huang, C., Lv, C., Zheng, C., Liu, D., Zhou, F., Huang, F., Hu, F., Ge, H., Wei, H., Lin, H., Tang, J., Yang, J., Tu, J., Zhang, J., Yang, J., Yang, J., Zhou, J., Zhou, J., Lin, J., Dang, K., Bao, K., Yang, K., Yu, L., Deng, L., Li, M., Xue, M., Li, M., Zhang, P., Wang, P., Zhu, Q., Men, R., Gao, R., Liu, S., Luo, S., Li, T., Tang, T., Yin, W., Ren, X., Wang, X., Zhang, X., Ren, X., Fan, Y., Su, Y., Zhang, Y., Zhang, Y., Wan, Y., Liu, Y., Wang, Z., Cui, Z., Zhang, Z., Zhou, Z., and Qiu, Z. Qwen3 technical report, 2025. URL <https://arxiv.org/abs/2505.09388>.
- Yang, D., Wang, D., Guo, H., Chen, X., Wu, X., and Meng, H. M. SimpleSpeech: Towards simple and efficient text-to-speech with scalar latent transformer diffusion models. *ArXiv*, abs/2406.02328, 2024. URL <https://api.semanticscholar.org/CorpusID:270226637>.
- Yao, J., Jacobs, S. A., Tanaka, M., Ruwase, O., Subramoni, H., and Panda, D. K. Training ultra long context language model with fully pipelined distributed transformer, 2025. URL <https://arxiv.org/abs/2408.16978>.
- Zhao, Y., Gu, A., Varma, R., Luo, L., Huang, C.-C., Xu, M., Wright, L., Shojanazeri, H., Ott, M., Shleifer, S., Desmaison, A., Balioglu, C., Damania, P., Nguyen, B., Chauhan, G., Hao, Y., Mathews, A., and Li, S. Pytorch fsdp: Experiences on scaling fully sharded data parallel, 2023. URL <https://arxiv.org/abs/2304.11277>.

A. Appendix

A.1. Single Node Memory Comparisons

Table 4. **Memory comparison** (GiB) for **Llama3-8B** ($8\times H100s$) and **Qwen3-32B** ($16\times H100s$) across varying sequence lengths. UPipe processes attention in a headwise chunked manner, reducing peak memory usage during training. This leads to practical advantage of longer sequence length support on Llama3-8B (upto 5M tokens), improving by 25% over prior SOTA (FPDT: 4M tokens). **OOM**: Out of Memory. **Note**: FPDT execution fails at lengths $> 4M$.

	Model	128K	256K	512K	1M	2M	3M	4M	5M
Llama3-8B	Native-PyTorch	25.32	31.40	43.55	67.86	OOM	–	–	–
	Ring	21.32	23.40	27.58	35.86	52.49	69.11	OOM	–
	Ulysses	21.26	23.02	26.80	34.35	49.49	64.55	OOM	–
	FPDT	21.73	22.50	24.03	27.09	35.17	43.35	51.42	–
	UPipe	21.10	22.30	24.70	29.90	40.50	51.10	61.70	72.30
Qwen3-32B	Native-PyTorch	45.81	53.69	69.47	OOM	–	–	–	–
	Ring	40.14	41.16	44.22	50.51	63.11	OOM	–	–
	Ulysses	40.13	41.16	44.10	50.27	62.60	OOM	–	–
	FPDT	38.94	39.47	40.54	42.66	46.91	52.27	57.77	–
	UPipe	39.98	40.84	42.72	46.84	55.65	64.47	73.28	OOM

Table 4 shows the memory comparison of various context parallelism schemes on Llama3-8B and Qwen3-32B models across different context lengths. FPDT shows best memory usage due to arbitrary chunk size setting, but performs poorer due to CPU overheads. UPipe has better memory efficiency than all other methods, while also matching the throughput with respect to Ulysses. Note that while FPDT reports lower allocated memory, it is unable to run with context length $> 4M$.

A.2. Runtime comparison between DS-Ulysses and UPipe

Table 5. **Runtime comparison** (in seconds) for **Llama3-8B** on $8\times H100$ between DS-Ulysses and UPipe across varying sequence lengths. **FA3-Fwd/Bwd**: Total flash-attention-3 forward and backward kernel time. The runtime refers to the total time for a single training step.

		128K	256K	512K	1M	2M	3M
DS-Ulysses	All-to-All	0.40	0.90	1.68	4.93	16.30	42.21
	FA3-Fwd	1.58	6.35	25.71	103.49	421.67	995.92
	FA3-Bwd	2.40	9.13	36.74	146.86	588.73	1324.71
	Other	3.03	5.33	10.08	19.78	41.30	56.31
	Total	7.40	21.72	74.21	275.06	1068.00	2419.14
UPipe	All-to-All	0.46	1.10	2.43	5.52	17.12	34.34
	FA3-Fwd	1.51	6.38	25.93	103.92	417.55	940.62
	FA3-Bwd	2.41	9.25	36.99	147.37	590.79	1330.76
	Other	2.82	5.23	10.10	19.58	37.76	55.52
	Total	7.20	21.96	75.45	276.39	1063.23	2361.24

Table 5 shows the runtime comparison for Llama3-8B on a single $8\times H100$ node for DS-Ulysses and UPipe. It shows the breakdown of runtime into major components of a single training step: flash-attention-3 forward time, flash-attention-3 backward time, and All-to-All communication time. Note that UPipe has higher runtime at lower sequence lengths due to multiple kernel launches. However, this is amortized at higher sequence lengths due to enough work per kernel launch saturating the GPU.

A.3. GQA backward-attention memory

Table 6. Peak activation memory within the backward attention block under GQA. Note: π represents the number of chunks in FPDT, ν represents the number of chunks in UPipe. As shown, UPipe consumes ν times lesser intermediate (QKV + all-to-all) tensor memory than Ulysses + offloading. FPDT has lower memory usage due to arbitrary chunk size, but suffers from performance degradation.

Method	Before Bwd Attn	During out_all_to_all	During Bwd Attn Kernel	During inp_all_to_all
Ulysses	$(L + 1) \frac{S}{C}$	$(L + 2) \frac{S}{C}$	$(L + \beta + 1) \frac{S}{C}$	$(L + \gamma + 1) \frac{S}{C}$
Ulysses + offloading	$2 \frac{S}{C}$	$3 \frac{S}{C}$	$(\beta + 2) \frac{S}{C}$	$(\gamma + 2) \frac{S}{C}$
FPDT	$\frac{S}{C \cdot \pi}$	$3 \frac{S}{C \cdot \pi}$	$(\beta + 2) \frac{S}{C \cdot \pi}$	$(\gamma + 2) \frac{S}{C \cdot \pi}$
Untied Ulysses	$2 \frac{S}{C}$	$2 \frac{S}{C} + 2 \frac{S}{C \cdot \nu}$	$2 \frac{S}{C} + (\beta + 1) \frac{S}{C \cdot \nu}$	$2 \frac{S}{C} + 2(\gamma + 1) \frac{S}{C \cdot \nu}$